POLITECNICO DI TORINO
Repository ISTITUZIONALE

Corrosion morphology of prestressing steel strands in naturally corroded PC beams

(Article begins on next page)

28 April 2024

Corrosion Morphology of Prestressing Steel Strands in Naturally Corroded PC Beams

Francesca Vecchi
Department of Engineering and Architecture, University of Parma,
Parco Area delle Scienze 181/A, 43124 Parma, Italy
Tel: +390521905930, Fax: +390521905924
francesca.vecchi@unipr.it

Lorenzo Franceschini
Department of Engineering and Architecture, University of Parma,
Parco Area delle Scienze 181/A, 43124 Parma, Italy
Tel: +390521905930, Fax: +390521905924
lorenzo.franceschini@unipr.it

Francesco Tondolo
Department of Structural, Geotechnical and Building Engineering, Politecnico di Torino,
Corso Duca degli Abruzzi 24, 10129 Turin, Italy
francesco.tondolo@polito.it

Beatrice Belletti *(corresponding author)*
Department of Engineering and Architecture, University of Parma
Parco Area delle Scienze 181/A, 43124 Parma, Italy
Tel: +390521905930, Fax: +390521905924
beatrice.belletti@unipr.it

Javier Sánchez Montero
Institute Eduardo Torroja of Construction Sciences, Serrano Galvache, Madrid, Spain
javier.sanchez@csic.es

Paolo Minetola
Department of Management and Production Engineering, Politecnico di Torino, Turin, Italy
Corso Duca degli Abruzzi 24, 10129 Turin, Italy
paolo.minetola@polito.it

Abstract

The geometric morphology of pits induced by corrosion has been investigated. To this aim, twenty-four seven-wire strands coming from 10 years old naturally corroded prestressed concrete beams have been analysed. The cross-sections of corroded strands were measured and examined in detail. The morphology of corrosion pits has been recorded by using a structured light 3D scanner and classified in terms of maximum pit depth, longitudinal dimension, and transversal width. Then, a new method for the approximate evaluation of the average pit depth of prestressing strands has been proposed. Finally, the pitting factor of the corroded samples has been calculated.

1   INTRODUCTION

Currently, steel corrosion has been worldwide considered as one of the primary reasons for durability deterioration in reinforced (RC) and prestressed (PC) concrete structures. In the last thirty years, the detrimental effects of the corrosion process have been deeply investigated by many authors and have been generally identified in the formation of rust products, loss of cross-sectional area, [1],[2], reduction of mechanical properties [3], and reduction of bond [4]. In this context, spalling of concrete, delamination, cracking and more relevant issues, such as reduction of serviceability and ultimate resistance have been regarded as the main consequences of corrosion deterioration [5]-[8].

It should be noted that pitting corrosion is the major corrosion mechanism in corroded strands in marine environments [9]-[11]. Chlorides break the passive layer locally and pits growing may cause the cross-sectional area reduction of the wires [12], [13], the stresses concentration, and the fracture localization [14], [15]. As a result, a relevant reduction of safety margin can be observed. In addition, since prestressing technology is a widely technique adopted in bridges and relevant infrastructures, particular attention should be devoted to the evaluation of chloride-induced corrosion in this type of structures. Some historical bridge collapses, such as the Ynys-y-gwas bridge in Port Talbot [3], the Saint Stefano bridge in Italy [16], and the pedestrian bridge at Lowe's Motor Speedway in North Carolina [17], brought the problem to the scientific attention [18] and addressed the ongoing research on the evaluation of the structural durability of PC members characterised by pitting corrosion.

Despite a large amount of works has been carried out on pitting corrosion of reinforcing steel [19]-[28], minor attention has been paid to prestressing strands or wires. However, the effect of corrosion on the mechanical behaviour of strand should be studied to prevent possible catastrophic failures and to generally ensure the structural safety of existing structures and infrastructures. In this regard, Yoo et al. [29] examined naturally corroded seven-wire strands belonging to two in-service bridges. Based on the obtained results, they developed a method for the estimation of the section loss. Darmawan and Stewart [30] carried out accelerated corrosion tests on prestressing wires, leading to a probabilistic model for the prediction of the depth and the variability of pitting in case of pretensioned prestressing wires.

Limited studies have been carried out on the investigation of the corrosion morphology of strand, which is a fundamental feature for the estimation of its residual strength capacity. In general, a simplified hemispherical pit configuration is assumed for the definition of analytical damage models for the prediction of the stress-strain relationship of corroded prestressing strands [3],[31]. On the other hand, ellipsoid shape of the pit is commonly adopted in numerical investigations [32]-[33]. Recently, Jeon et al. [34] defined three types of pit configurations for the description of the shapes of corroded strands, based on the measured maximum pit depth. However, as pointed out by Wang et al. [35], irrational results could be obtained when the morphology of pits is not completely defined through the evaluation of both depth and width. To this aim, Wang et al. [35] carried out an experimental campaign by analysing a total of 119 pits coming from prestressing strands artificially corroded. The authors classify the pit as spheroidal, saddle and pyramidal. The effect of the pit's morphology in case of wires on the performance of existing structures represents an interesting research topic for the determination of the relevant parameters for design and maintenance procedures of Guidelines and Codes.

Indeed, the correct definition and interpretation of pits configuration leads to the prediction of the stress-strain relationship of corroded prestressing strands. Even if different decay laws have been proposed by several authors (Lu et al. [3], Jeon et al. [34], Wang et al. [35], and Zhang et al. [36]) to

2

95 describe the mechanical properties of corroded prestressing strands, the complexity of the problem re-
96 quires further investigation. These methods for the estimation of mechanical performances of corroded
97 prestressing strands are based on mass loss and exposed time. However, since the measurement of the
98 mass loss requires destructive testing, they suffered by limited applicability during in-situ inspection.
99 On the other hand, the identification of the most corroded section and the measurement of the maximum
100 pit depth along the entire length of the strand by using adequate equipment, as the pit depth gauge, are
101 easily assessable during non-destructive testing. In order to provide useful tools for the in-situ inspec-
102 tion of in-service structure, new correlations between maximum pit depth and mass loss for different
103 levels of corrosion are proposed in this paper.

104 Additionally, the outcomes of the present work provide data for a reliable calibration of existing
105 models or novel insights for the development of new methods for the evaluation of corrosion effects in
106 prestressing strands. For example, Lu et al. [3] and Jeon et al. [34] proposed a model of micro-spring
107 damage unit, which describes the equivalent stress-strain model of a corroded strand through the be-
108 haviour of seven springs, that represent each wire, placed in parallel. Based on this assumption, the
109 failure of the strand is reached when the rupture of the first wire takes place, Figure 1. Thus, the correct
110 determination of the minimum residual cross-sectional area of the most corroded wire plays a funda-
111 mental role in defining the mechanical behaviour of the whole strand. In particular, the response of a
112 corroded strand cannot exclude an accurate description of the morphology of corrosion pits.
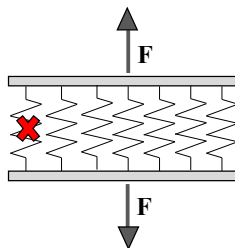

113
114   Figure 1. Spring model of a corroded strand.

115 In this context, the estimation of the overall level of corrosion is generally carried out considering the
116 average corrosion depth only. However, the evaluation of this quantity might lead to an overestimation
117 of the load bearing capacity of corroded elements [37]. Therefore, in order to provide a relationship
118 between local and general corrosion damage, expressed by the maximum pit depth and the average
119 corrosion depth, respectively, the pitting factor, P_f, has been investigated. The pitting factor, P_f, is de-
120 fined as the ratio between the maximum pit depth and the average corrosion depth. Furthermore, based
121 on the discrepancy observed in previous research on RC members [19]-[24], widespread dispersion of
122 this factor has been recorded. For example, Tuutti [19] found out a pitting factor range varying from 4
123 to 10, while the results provided by Gonzalez et al. [21] ranged from 2.7 to 8.9 and from 5.9 to 16.1 in
124 case of natural corrosion and accelerated corrosion, respectively. To the authors' knowledge, the study
125 conducted by Darmawan and Stewart [30] is the only one that have examined the pitting factor in case
126 of prestressing wires subjected to accelerated corrosion process, recording a range varying from 8.5 to
127 10.9. Thus, the present work aims to investigate for the first time the fluctuation of the pitting factor in
128 naturally corroded prestressing strands providing more reliable data.

129 To this aim, twenty-four seven-wire strands coming from 10 years old naturally corroded PC beams
130 were retrieved from low stressed parts after the failure tests performed on the beams. The cross-sections
131 of naturally corroded seven-wire strands were measured and examined in detail. The morphology of
132 corrosion pits has been analysed by using a structured light 3D scanner and classified in terms of max-
133 imum pit depth, longitudinal dimension, and transversal width. Finally, a new step-by-step method for
134 the approximate evaluation of the average pit depth of prestressing strands, for any corrosion rate, has
135 been proposed. Thus, the method presented in this study, which is based on the correlation between
136 maximum pit depth and the measured mass loss, is expected to provide useful information to research-
137 ers and engineers who investigate the structural safety and the maintenance of corroded strands.

138   **2   MATERIALS and METHODS**

139   **2.1   Specimens**

In order to extend the experimental data available in the scientific literature, as well as analyse the residual capacity and failure modes of full-scale corroded prestressed concrete (PC) beams, six naturally corroded PC beams were tested at the "Instituto de Ciencias de la Construcciòn Eduardo Torroja" in Madrid from March to June 2019. The outcomes of the study were recently published by Belletti et al. [11] and Vecchi et al. [38], investigating the residual shear and flexural capacity of the tested beams, respectively.

The PC beams came from a refrigeration tower of a thermal power plant, where refrigeration wetting cycles using seawater were repeated over time. Chloride-induced corrosion was observed after 10 years of service life.

The specimens were 5210 mm long and were characterised by a transversal cross-section of width, b, equal to 150 mm and height, h, equal to 300 mm, Figure 2. The bottom prestressing reinforcement consisted of two seven-wires strands 1/2S - having an equivalent diameter equal to 12.9 mm-, while two ribbed bars - having an equivalent diameter equal to 5 mm - characterised the top reinforcement. Table 1 briefly reports the uncorroded mechanical properties of strands and rebars, respectively.
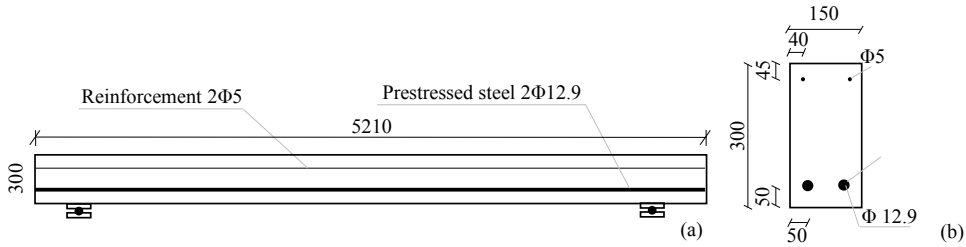

Figure 2. Geometrical features of the beams [in mm]: (a) Longitudinal view and (b) Transversal cross-section.

Table 1. Mechanical properties of strands and rebars: (a) Longitudinal view and (b) Transversal cross-section.

Type of Reinforcement	Yield Strength [MPa]	Ultimate Strain [%]	Modulus of Elasticity [MPa]
Strands	1580	5	$195 \cdot 10^3$
Rebars	435	18	$200 \cdot 10^3$

After three-point shear and four-point bending tests, a total of 24 prestressing strands were retrieved from the tested PC beams. Thereafter, two groups of twelve samples were collected: the first group was characterised by samples 450 mm long, Figure 3(a), while the other by samples 700 mm long, Figure 3(b).

2.2   Measurement and Post-processing Procedure

In general, the entire procedure, which will be deeply discussed in the following paragraphs, consisted of seven main phases: (I) classification of strands by carrying out an external visual inspection; (II) to (IV) evaluation of the mass loss, η; (V) 3D scanning of samples by using a structured light scanner of the GOM ATOS series; (VI) analysis of the pit location, dimensions, and distribution by importing data in GOM Inspect software (release 2019); (VII) to (VIII) post-processing analysis and discussion of the obtained results.
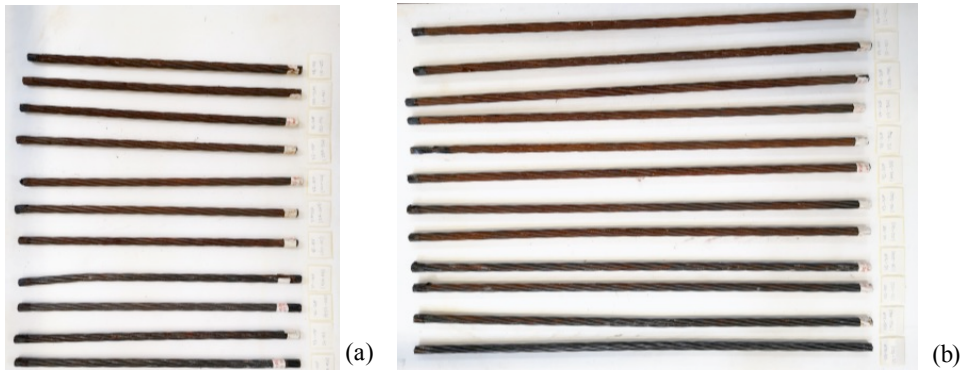
Figure 3. Samples: (a) 450 mm long, and (b) 700 mm long.

3   THEORY and CALCULATIONS

3.1   Visual Inspection

After the failure tests, the prestressing strands were extracted and initially classified through a visual inspection carried out with naked eye. To this aim, the strands were subdivided in pieces 500 mm long. The low level was characterised by the presence of small and localised pits, the medium level presented bigger and widespread pits, while the high level of corrosion was identified by the presence of deeper and oversize pits, covering a large region of the external wire surface, and showing a relevant rust products formation, Table 2.

Successively, a second classification, based on the samples mass loss, η, has been conducted. The procedure adopted for the evaluation of the mass loss is described in section 3.2. According to Lu et al. [3], three levels of corrosion have been considered, which correspond to three ranges of measured mass loss, η. The lower level of corrosion, LV-I, represents mass losses ranging from 0 to 2%; the medium level, LV-II, stands for mass losses ranging from 2% to 10%, while the highest level, LV-III, refers to mass losses higher than 10%, Table 2.

Table 2. Corrosion level, mass loss range, and reference samples for visual inspection classification.

Corrosion Level	Mass Loss Range	Samples
LV-I	$\eta \leq 2\%$	
LV-II	$2\% < \eta \leq 10\%$	
LV-III	$\eta > 10\%$	

The samples were collected using an identifying code where PB stands for prestressed beam followed by a number varying from 9 to 14 indicating the name of the reference beam; the letter L or R is introduced to specify the left or right strand cross-section position, while numbers in brackets represent the initial and final abscissa at which the sample was retrieved and provide information about its length. Table 3 reports the 24 samples classification by listing the identifying code, the reference beam, the sample length, L_i, and the associated level of corrosion attributed *via* visual inspection.

Table 3. Classification of the samples.

Identifying Code	Beam	L_i [mm]	Level of corrosion Visual Inspection	η [%]	Level of corrosion Gravimetrical Method
PB9-L(12-82)	PB4P9	700	LV-III	17.3	LV-III
PB9-L(426-496)	PB4P9	700	LV-I	2.8	LV-II

5

PB9-R(15-60)	PB4P9	450	LV-III	21.5	LV-III
PB9-R(428-473)	PB4P9	450	LV-I	1.7	LV-I
PB10-L(138-208)	PB3P10	700	LV-I	2.4	LV-II
PB10-L(445-515)	PB3P10	700	LV-II	6.3	LV-II
PB10-R(32-102)	PB3P10	700	LV-I	2.2	LV-II
PB10-R(287-332)	PB3P10	450	LV-III	8.0	LV-II
PB11-L(5-75)	PB3P11	700	LV-I	2.7	LV-II
PB11-L(196-266)	PB3P11	700	LV-II	2.9	LV-II
PB11-R(6-51)	PB3P11	450	LV-I	2.0	LV-I
PB11-R(273-318)	PB3P11	450	LV-I / LV-III	4.8	LV-II
PB12-L(12-82)	PB3P12S	700	LV-III	14.2	LV-III
PB12-L(124-169)	PB3P12S	450	LV-II	4.3	LV-II
PB12-R(100-170)	PB3P12S	700	LV-II	5.3	LV-II
PB12-R(358-403)	PB3P12S	450	LV-I	1.4	LV-I
PB13-L(1-46)	PB4P13	450	LV-III	7.6	LV-II
PB13-L(108-178)	PB4P13	700	LV-II	4.3	LV-II
PB13-R(0-70)	PB4P13	700	LV-II / LV-III	11.4	LV-III
PB13-R(70-115)	PB4P13	450	LV-II	4.6	LV-II
PB14-L(10-55)	PB4P14	450	LV-III	14.7	LV-III
PB14-L(455-500)	PB4P14	450	LV-I	0.03	LV-I
PB14-R(2-72)	PB4P14	700	LV-II / LV-III	11.6	LV-III
PB14-R(77-122)	PB4P14	450	LV-II	3.8	LV-II

3.2 Mass Loss Evaluation

After the visual inspection, the strands were weighed by using a digital scale, which has an accuracy of 0.01 g. The sample PB14-L(455-500) has been assumed as reference sample and considered uncorroded, since it showed the highest recorded weight per unit length, m_{nc}, equal to 0.7994 g/mm.

The uncorroded mass of the samples, m_0, has been obtained by the product between the uncorroded weight per unit length, m_{nc}, and the length of the analysed sample, L_i, as expressed in Eq. (1):

$$m_0 = m_{nc}L_i \qquad (1)$$

Then, according to the method specified by ASTM G1-03 [40], the cleaning phase was carried out and the mass loss, η, has been calculated through Eq. (2) and reported in Table 3:

$$\eta = \frac{m_0 - m}{m_0}100 \qquad (2)$$

where m is the residual mass of sample neglecting the weight loss due to rust products and obtained by using Eq. (3):

$$m = m_0 - \Delta_{TOT} = m_0 - (\Delta_1 + \Delta_2) \qquad (3)$$

where Δ_{TOT} is the total weight loss, calculated as the sum between the weight loss due to first handling, Δ_1, and the weight loss due to cleaning procedure, Δ_2. Based on ASTM G1-03 [40], the variation of weight loss during the cleaning procedure was graphed as a function of the number of equal cleaning cycles, as showed in Figure 4 for sample PB11-R(6-51). Two lines AB and BC, with different slopes, can be geometrically plotted interpolating the weight loss variation, Δ_i, calculated at each cleaning cycle. In the beginning, because a huge quantity of rust products was removed, the weight loss was relevant - line AB. After the second cleaning cycle, a sizeable change in the slope angle, due to a reduction in the weight loss variation, Δ_i, was observed - line BC. As a result, the weight loss, Δ_2, due to the cleaning procedure was identified by the intersection point, B, of lines AB and BC, as highlighted by the triangular red marker in Figure 4.
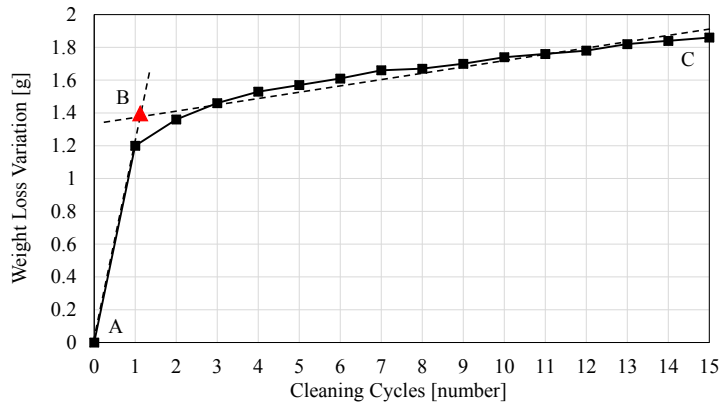
Finally, the correspondence of the estimated level of corrosion - established via visual inspection - and the calculated one - obtained by comparing the measured mass loss, η, with the ranges associated with the three levels of corrosion previously assumed in paragraph 3.1 - has been assessed and reported in Table 3. In general, good correspondence has been observed. In few cases, as for example PB10-L(138-208) and PB10-R(32-102), the measured mass loss was in proximity to the upper or lower bound of the level of corrosion established *via* visual inspection.

3.3   Three-Dimensional Scanning

Before the scanning phase, samples should be carefully set up. Firstly, the sample surface was cleaned. Then, a custom-made fixture was used to easily position the sample in the working volume of the 3D scanner. The fixture comprises a metal support plate (Figure 5a) and two 3D printed bearings of ABS material. The two bearings can be moved along the support plate to fit the sample length of 450 or 700 mm. They are used to rotate the sample around its longitudinal axis during the scanning activity. Some octagonal base prisms, hereafter called "reference supports", have been 3D printed using a PLA filament (Figure 5c). The final configuration of the fixture, placed below the 3D scanner, is shown in Figure 5a.
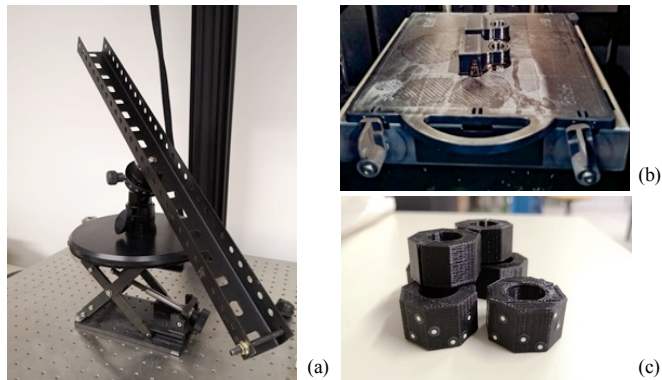
Figure 5. Support elements: (a) metal support plate, (b) 3D printed bearings, and (c) octagonal base prisms.

The actual morphology of the samples is retrieved using an ATOS Compact structured light 3D scanner. The ATOS scanner exploits stereoscopic vision using two 2-megapixel cameras and the triangulation principle to measure the 3D coordinates of points on the surface of the sample through fringe projection with blue LED light, Figure 6.

The working volume of the ATOS Compact scanner is 125 mm x 90 mm x 90 mm and its length measurement error is smaller than 0.020 mm according to the acceptance test of VDI/VDE 2634 Part 3 guideline. Round adhesive markers of 1.5 mm diameter with a central white circle are placed on the

7

faces of the octagonal prims to create a network of fixed reference points that are used by GOM scan software to automatically align the data of multiple scans in the same cartesian reference frame.

Before scanning, a thin white layer of opaque anti-reflection agent Metal Service MR® 2000 Anti-Reflex L was applied on the sample surface. The agent is used to reduce the reflection that is typical of metal surfaces and to enhance the contrast of the sample in the images acquired by the cameras of the 3D scanner. It has been demonstrated that the application of the anti-reflection agent does not alter the optical measurements significantly, [39].
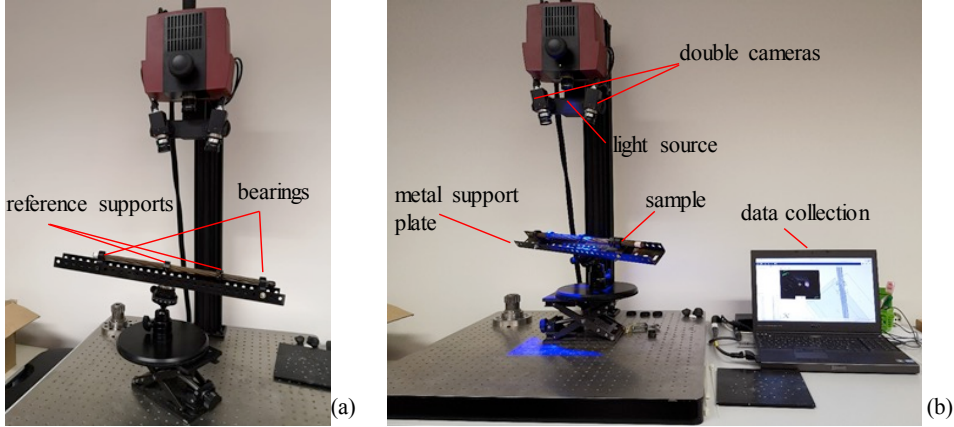

Figure 6. Structured light scanning system: (a) final configuration and (b) scanning phase.

In the present work, the entire length of the strand might be scanned. However, since the presence of the gripping system has been predicted in the following tensile tests, a length equal to 100 mm at both strand edges has been neglected during the scanning phase. Based on this assumption, the scanned length for the two analysed groups of samples (450 mm and 700 mm) has been equal to 250 mm and 500 mm, respectively. Additionally, only the external surface of the six external wires have been scanned, assuming the hidden surfaces of the external wires and the central straight wire as uncorroded. This assumption has been confirmed during the cleaning procedure.

The scanning phase returned as result a cloud of points scattered in space that has been converted by the scan software in tassellated surfaces using triangles. The virtual model of the real geometry of the sample was then exported using the STL format, Figure 7(a).

3.4 Post-processing of scan data

The last phase involved the post-processing of data. Once the scanning phase was completed, the STL file of each sample has been imported in GOM Inspect software for the comparison with the uncorroded reference sample PB14-L(455-500), Figure 7(b). Before comparison, the scan data of each sample was aligned to the reference one by using the best-fit algorithm of GOM Inspect software. This algorithm iteratively computes the roto-translation matrix to be applied to the compared data for minimization of the alignment and superposition error with respect to the reference data. The result of best fitting is shown in Figure 7, where the blue 3D model represents the reference sample. Figure 7(d) shows a detail of the recorded pits in the case of sample PB11-R(273-318).
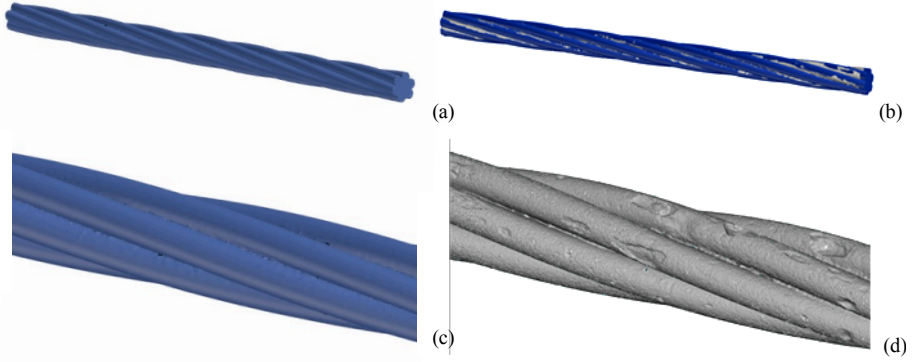
Figure 7. GOM Inspect software analysis: (a) uncorroded reference model, (b) alignment between un-corroded and corroded model, (c) detail of uncorroded sample PB14-L(455-500) and (d) detail of corroded sample PB11-R(273-318).

To obtain a general overview of the pitting corrosion deterioration along the entire scanned length of the samples, a detailed evaluation of the cross-section variation has been carried out every 10 mm by using GOM Inspect software. The measuring accuracy of GOM Inspect has been tested and certified by the German PTB institute and the American NIST Institute.

Basically, according to software outputs, the following interesting quantities can be obtained: (i) maximum pit depth, P_x, (ii) area of the pit, A_p, (iii) pit shape, P_y and P_z, (iv) number of pits and their distribution along the length of the scanned sample, (v) uncorroded cross-sectional area, A_0, (vi) average cross-sectional area, A_{av}, and (vii) minimum cross-sectional area, A_{min}.

The evaluation of pits depth, P_x, and the detection of the cross-sectional area of pits, A_p, have been obtained by the superposition of the corroded and the uncorroded samples, as shown in Figure 8 and in Figure 10(b). Furthermore, the pit shape in terms of longitudinal length, P_y, and transversal width, P_z, has been identified and measured, as highlighted in Figure 10(c).
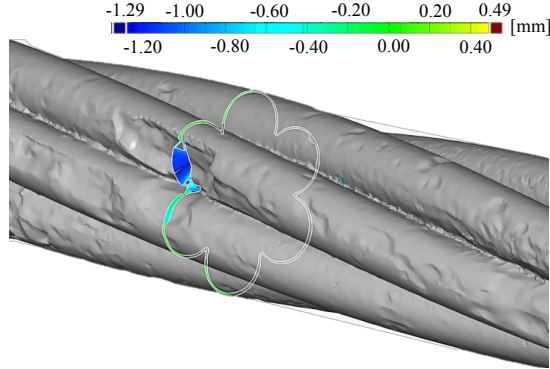
Figure 8. Example of cross-section analysis using GOM Inspect software in case of PB12-L(124-169).

The maximum pit of each external wire for the 24 collected seven-wire strands has been analysed in terms of P_x, P_y, and P_z. Furthermore, the pits were classified comparing the recorded pit area, A_p, with the loss of sectional area evaluated in accordance with the three pit configurations proposed by Jeon et al. [34] and shown in Figure 9, Eq.(4)-(6):

$$A_{p,1} = 2r^2 \left(\vartheta_1 - 2\sin\vartheta_1 \cos\vartheta_1 \right) \qquad \vartheta_1 = \arccos\left(1 - \frac{P_x}{2r} \right) \tag{4}$$

$$A_{p,2} = r^2 \left(2\vartheta_2 - \pi - 2\sin\vartheta_2 \cos\vartheta_2 \right) \qquad \vartheta_2 = \arccos\left(-\frac{P_x}{2r} \right) \tag{5}$$

9

$$A_{p,3} = r^2 \left(\vartheta_3 - \sin \vartheta_3 \cos \vartheta_3 \right) \qquad \vartheta_3 = \arccos\left(1 - \frac{P_x}{r} \right) \qquad (6)$$

where r is the radius of the external wire set equal to 2.13 mm, and θ_1, θ_2, θ_3 are the corrosion angles related to the different pit shapes, as shown in Figure 9. Figure 9 depicts the actual shape of corroded strands corresponding to the different types of pit's shapes, where the orange area is the residual cross-sectional area.

Table 4 reports the geometrical description and classification of the overall maximum pit recorded for the 24 collected samples, except for PB10-R(32-102), PB11-L(5-75), PB12-R(358-403), and PB14-L(455-500), where sizeable pits have not been detected. Additionally, during the scanning phase of PB11-R(273-318), errors due to optical occlusions have been observed, thus this sample has not been considered in the following. Hence, a total of 19 corroded samples have been deeply investigated. A more detailed description of the maximum pits detected for each external wire is reported in Appendix A.

Table 4. Maximum pit description and classification of the specimens.

Identifying Code	P_x [mm]	P_y [mm]	P_z [mm]	A_p [mm²]	$A_{p,1}$ [mm²]	$A_{p,2}$ [mm²]	$A_{p,3}$ [mm²]	Classification according to Jeon et al. [34]
PB9-L(12-82)	1.711	26.0	2.24	5.76	4.08	7.08	5.35	3
PB9-L(426-496)	0.424	0.73	0.83	0.51	0.53	1.80	0.74	1
PB9-R(15-60)	2.784	13.78	2.87	9.21	8.09	10.94	9.86	3
PB9-R(428-473)	0.169	1.86	0.65	0.11	0.14	0.72	0.19	1
PB10-L(138-208)	0.590	5.87	2.56	1.35	0.86	2.50	1.19	3
PB10-L(445-515)	2.447	8.39	3.56	7.78	6.76	9.80	8.46	3
PB10-R(32-102)	Uncor.	-	-	-	-	-	-	-
PB10-R(287-332)	2.880	10.17	2.95	8.41	8.47	11.24	10.24	1
PB11-L(5-75)	Uncor.	-	-	-	-	-	-	-
PB11-L(196-266)	1.402	8.75	3.09	4.38	3.06	5.86	4.08	3
PB11-R(6-51)	0.976	4.24	2.11	2.15	1.81	4.11	2.46	3
PB11-R(273-318)	Negle.	-	-	-	-	-	-	-
PB12-L(12-82)	1.55	15.47	3.89	4.82	3.54	6.44	4.68	3
PB12-L(124-169)	1.227	10.84	2.88	3.17	2.53	5.15	3.40	3
PB12-R(100-170)	1.001	6.8	2.29	1.98	1.88	4.22	2.55	1
PB12-R(358-403)	Uncor.	-	-	-	-	-	-	-
PB13-L(1-46)	1.161	6.44	2.23	2.50	2.33	4.88	3.15	1
PB13-L(108-178)	1.840	12.09	3	3.79	4.53	7.58	5.89	1
PB13-R(0-70)	1.380	10.39	2.39	3.19	2.99	5.77	4.00	1
PB13-R(70-115)	1.008	12.01	2.84	2.80	1.90	4.25	2.58	3
PB14-L(10-55)	2.237	17.51	3.43	5.92	5.97	9.06	7.57	1
PB14-L(455-500)	Uncor.	-	-	-	-	-	-	-
PB14-R(2-72)	1.227	10.19	2.32	2.63	2.23	4.74	3.02	3
PB14-R(77-122)	0.541	2.53	0.96	0.71	0.76	2.30	1.05	1

The number of pits varies depending on the level of corrosion of the strands. In particular, small and poorly spread pits have been recorded along the entire length of low corroded strands, Figure 11(a). As the level of corrosion increases, larger and more widespread pits have been detected, Figure 11(b) - Figure 11(c).

Figure 12 shows the pits distribution along the scanned length of PB12-L(124-169).
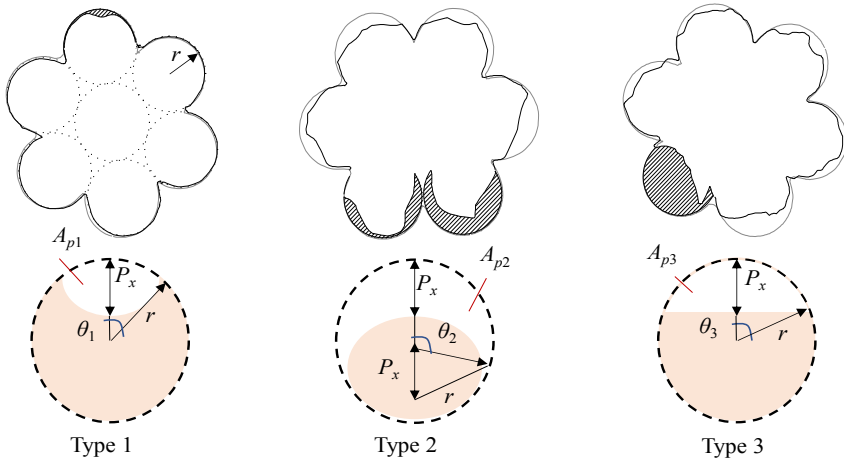
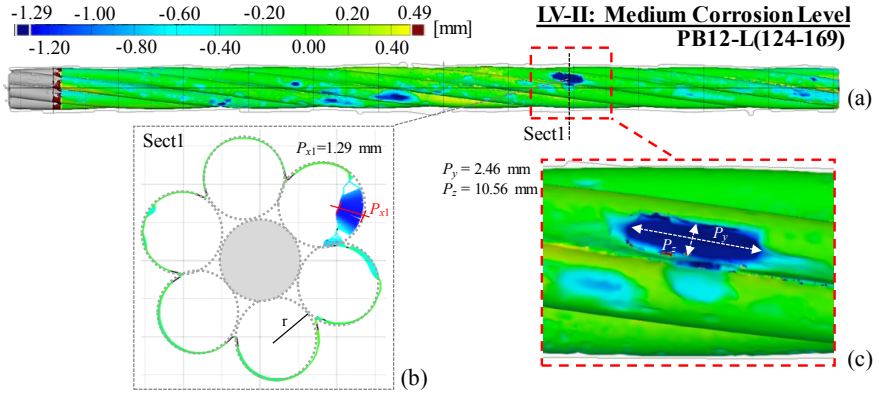Figure 9. Types of pit configuration according to Jeon et al. [34].

Figure 10. Pit configuration: (a) Scanned sample and pit identification, (b) cross-section and pit depth calculation, and (c) pit shape evaluation.
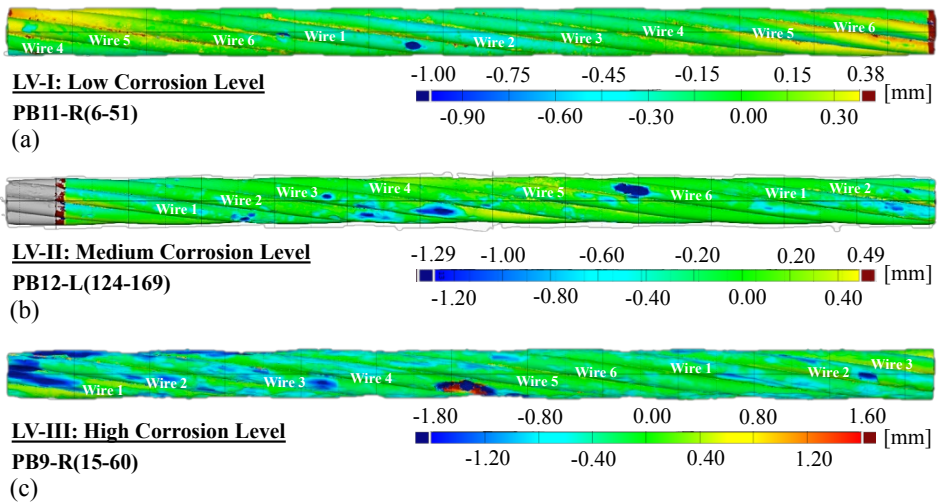
Figure 11. Number of pits for different levels of corrosion: (a) low, (b) medium, and (c) high level.

11
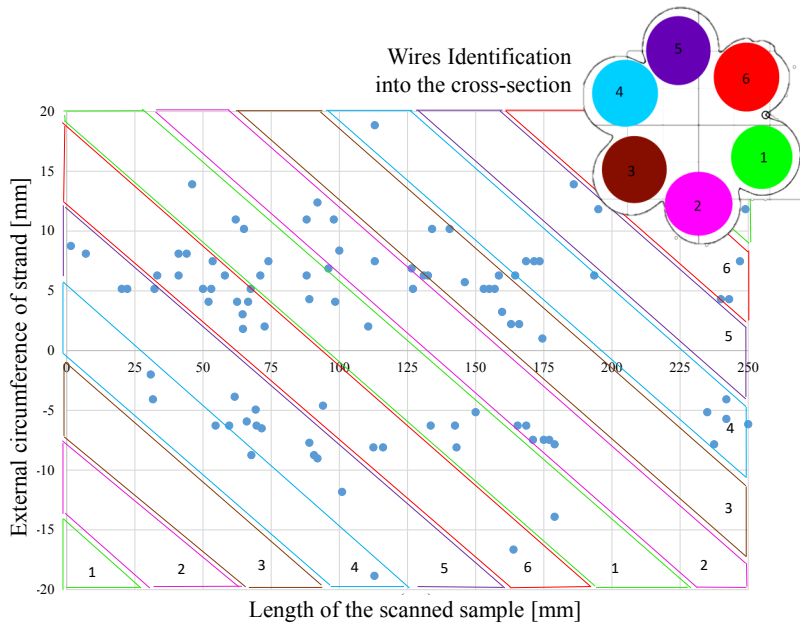
Figure 12. Pits distribution along the scanned length of sample PB12-L(124-169).

46.5% and 47.5% of the 101 recorded pits have been classified as type 1 and type 3, respectively, while the remaining 6% belongs to type 2. Type 2 pit configuration occurs in samples with mass loss higher than 10% - LV-III of corrosion. On the other hand, pits classified as type 1 and type 3 take place randomly, especially in the case of medium, LV-II, and high, LV-III, levels of corrosion. Neglecting the uncorroded strands, which show irrelevant pitting corrosion, only one sample, PB9-R(428-473), with a low level of corrosion ($\eta < 2\%$) has been characterised by type 1 pit configuration.

Figure 13 reports the relationship between the experimental maximum pit depth, P_x, and the relative area of the pit, A_p. The outcomes reveal that pits, classified as type 1 and type 3, are well fitted by the expressions provided by Eq.(4) and Eq.(6), respectively. On the other hand, a rough interpolation is obtained by using Eq.(5) for pits classified as type 2. Furthermore, as shown in Figure 13, the majority of pits is in a pith range varying from 0.5 mm to 1.5 mm with pit areas ranging from 0.5 mm^2 to 5.00 mm^2. Moreover, for pit depth higher than 1.6 mm, which is generally associated to high chloride-induced corrosion attack, only maximum pits belonging to type 1 and type 3 configurations have been recorded.

Figure 13. Relationship between pit depth and pit area.

338 Since, especially in case of a high level of corrosion, a similarity of type 1 and type 3 pit shapes has
339 been observed, a clear demarcation between these two configurations results hardly practicable during
340 in-situ inspection. Therefore, the single use of the type 3 configuration expression is proposed by the
341 authors for the classification of both pit typologies. In this regard, Figure 14 shows how the use of
342 Eq.(6) leads to a good interpolation of the experimental pits classified as type 1 and type 3. Considering
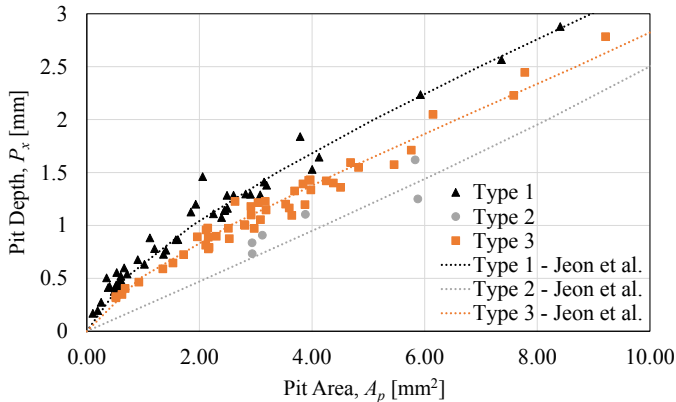343 only the maximum pits detected in the wires of the 19 corroded samples, Table 5 illustrates the percent-
344 age errors obtained in the calculation of the pit area, A_p, through the comparison of the experimental
345 results and the analytical outcomes using Eq.(6). In further detail, Appendix B reports the overall as-
346 sessment for each corroded wire. As a result, a general safe-side prediction of the pit area is obtained.
347 Additionally, referring to pits characterised by unsafe-predictions, the accuracy of the estimated value
348 - by using Eq.(6) - is confirmed by an average percentage error equal to 10.6%.

349
350
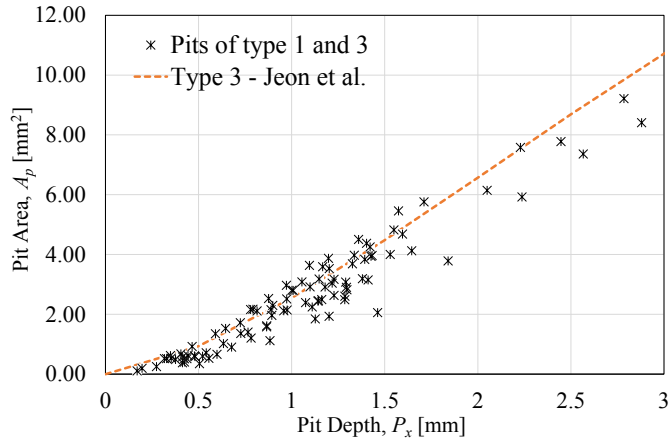
Figure 14. Experimental data fitting by using type 3 expression.

351
352

Table 5. Percentage error between experimental and analytical pit area, using type 3 expression.

Identifying Code	Wire	A_p [mm²]	Type 3 Jeon et al. [34]	
			Area [mm²]	Error [%]
PB9-L(12-82)	W_6	5.76	5.35	7.14
PB9-L(426-496)	W_4	0.51	0.74	-43.44
PB9-R(15-60)	W_4	9.21	9.86	-7.05
PB9-R(428-473)	W_4	0.11	0.19	-77.03
PB10-L(445-515)	W_4	7.78	8.46	-8.83
PB10-L(138-208)	W_3	1.35	1.19	11.39
PB10-R(287-332)	W_5	8.41	10.24	-21.87
PB11-L(196-266)	W_3	4.38	4.08	6.67
PB11-R(6-51)	W_1	2.15	2.46	-14.62
PB12-L(12-82)	W_1	4.82	4.68	3.00
PB12-L(124-169)	W_6	3.17	3.40	-7.23
PB12-R(100-170)	W_2	2.81	2.55	9.08
PB13-L(1-46)	W_5	2.50	3.15	-26.06
PB13-L(108-178)	W_3	3.79	5.89	-55.53
PB13-R(0-70)	W_5	3.19	4.00	-25.15
PB13-R(70-115)	W_2	2.80	2.58	7.91
PB14-L(10-55)	W_4	5.92	7.57	-27.86
PB14-R(2-72)	W_3	2.63	3.40	-29.19
PB14-R(77-122)	W_6	0.71	1.05	-47.43

353
354

13

4 RESULTS and DISCUSSION

4.1 Pit depth and cross-section distribution along sample length

For each collected strand, the pit depth variation along its length has been recorded by using GOM Inspect software. Figure 15 shows the longitudinal distribution of pit depth for four samples characterised by different levels of corrosion, η: (i) 2% for PB11-R(6-51), (ii) 4.3% for PB12-L(124-169), (iii) 8% for PB10-R(287-332), and (iv) 21.5% for PB9-R(15-60). As shown in Figure 15, even if pits occurred everywhere along the corroded sample length, the corresponding pit depth is not uniformly distributed and may differ considerably in adjacent cross-sections. This outcome confirms the scientific literature, which supports the randomness of chloride-induced corrosion in concrete. In particular, as reported by other authors [27],[41],[42] in case of reinforcing steel bars subjected to chloride attack, the pit depth is found to increase with the increased level of corrosion. In this regard, the maximum recorded pit depth, P_x, is 1 mm, 1.29 mm, 1.54 mm, and 1.95 mm in case of samples with mass loss equal to 2%, 4.3%, 8%, and 21.5%, respectively.

Irregular trends are also observed in terms of longitudinal distribution of the residual cross-sectional area, as reported in Figure 16. Referring to the uncorroded sample, the detected cross-sectional area, recorded by the structured light scanner, has been equal to 106.9 mm^2. The difference with the nominal area of 1/2S strand, which is equal to 99 mm^2, is due to the inability of the 3D scanner of measuring the empty spaces between wires. Similarly to pit depth, the residual cross-sectional area decreases with the increased level of corrosion. The minimum recorded cross-sectional area is 105.8 mm^2, 100.6 mm^2, 92.8 mm^2, and 84.0 mm^2 in the case of samples with measured mass loss equal to 2%, 4.3%, 8%, and 21.5%, respectively. According to the obtained results, it is possible to state that the residual cross-sectional area distribution along the strand length is random, consequently a univocal correlation with the maximum pit depth cannot be stated. In this regard, the maximum pit depth, P_x, has not been always detected in correspondence of the minimum residual cross-sectional area, A_{min}. For example, the maximum pit depth of sample PB9-R(15-60), which is 1.95 mm, occurred at an abscissa, x, equal to 110 mm, while the minimum cross-sectional area, equal to 84.0 mm^2, has been recorded at 0 mm.
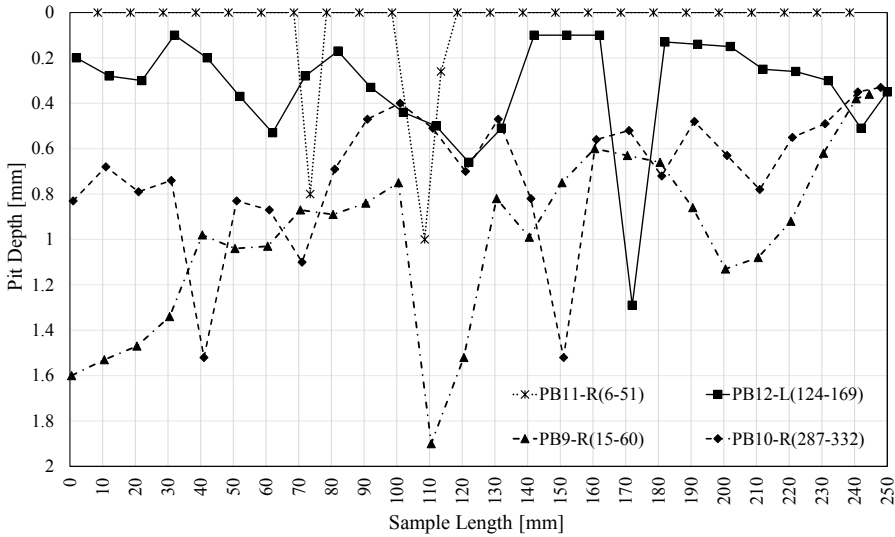
Figure 15. Distribution of pit depth along the length of samples: PB11-R(6-51) mass loss 2%, PB12-L(124-169) mass loss 4.3%, PB10-R(287-332) mass loss 8%, PB9-R(15-60) mass loss 21.5%.
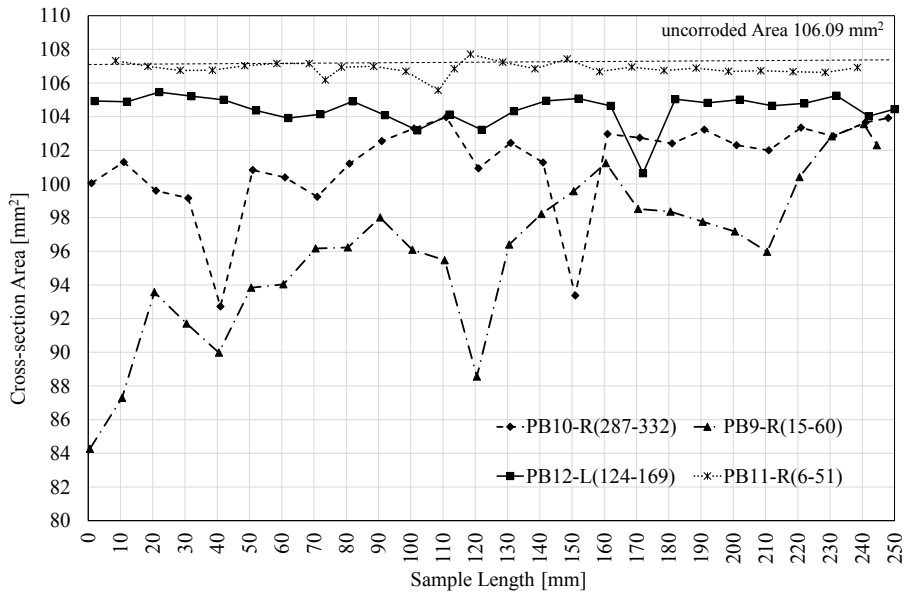
384
385 Figure 16. Distribution of residual cross-sectional area along the length of corroded samples: PB11-R(6-51) mass
386 loss 2%, PB12-L(124-169) mass loss 4.3%, PB10-R(287-332) mass loss 8%, PB9-R(15-60) mass loss 21.5%.

387 The evidence of the previous assessments is obtained by comparing three samples (PB14-L(10-55),
388 PB14-R(2-72), and PB14-R(77-122)) belonging to the edge region of beam PB4P14. Figure 17 high-
389 lights the randomness of pits in terms of both longitudinal distribution and maximum pit depth. In
390 particular, even if PB14-L(10-55) and PB14-L(2-72) are characterised by LV-III of corrosion, the min-
391 imum residual cross-sectional areas, equal to 88.5 mm^2 and 93.5 mm^2, and the positions, equal to 1.98
392 mm and 1.2 mm, at which the maximum pit has been detected are different. The results demonstrate
393 that the residual cross-sectional area distribution along the sample length is also a random variable.
394
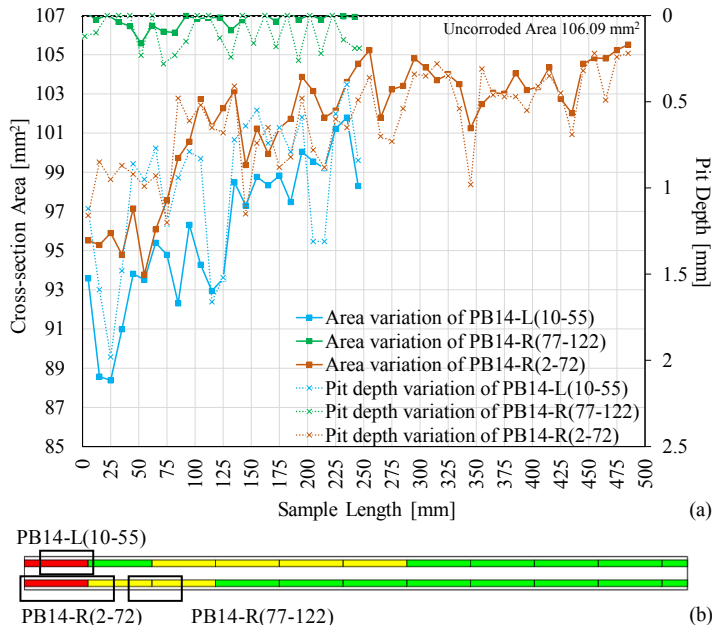
395
396 Figure 17. Distribution of maximum pit depth and residual cross-sectional area in case of beam PB4P14: (a) Com-
397 parison, and (b) position of the samples.

15

4.2 Mass loss vs maximum pit depth and minimum cross-sectional area

To deeply discuss and analyse the chloride-induced corrosion damages, a correlation with the mass loss, η, and the maximum pit depth, P_x, has been investigated. In this context, Figure 18 shows the relationship between the maximum pit depth and the mass loss percentage for the corroded samples and for the three levels of corrosion previously introduced in paragraph 3.1. Referring to the calculated mass loss evaluated according to the method specified by ASTM G1-03 [40], the maximum pit depth, P_x, can be analytically estimated. By performing a linear regression analysis three expressions are obtained for the three levels of corrosion, Eq.(7)-(9):

LV-I $\qquad\qquad\qquad\qquad P_x = 0.0601\eta$ $\qquad\qquad\qquad\qquad$ (7)

LV-II $\qquad\qquad\qquad\qquad P_x = 0.2804\eta$ $\qquad\qquad\qquad\qquad$ (8)

LV-III $\qquad\qquad\qquad\qquad P_x = 0.1206\eta$ $\qquad\qquad\qquad\qquad$ (9)

All the data have been fitted with the best function possible with respect to the linear regression coefficient, R^2. In particular, as shown in Figure 18, a widespread dispersion of the results with respect to the linear correlation trend is observed in the case of samples characterised by LV-I and LV-II of corrosion. For mass loss lower than 2%, the scatter of the results is probably related to the small number of samples. In this regard, further studies are needed in order to extend the available data of samples with a low level of corrosion. Considering the second range, the dispersion of the results was observed also in case of reinforcing rebars. Li et al. [27] highlighted that the maximum pit depth can better reflect the severity of local corrosion, while the mass loss is more suitable for representing the average corrosion level. Indeed, widespread small pits with low values of maximum pit depth or limited and deep pits with high values of maximum pit depth can return the same mass loss. On the other hand, a good interpolation is carried out in case of LV-III of corrosion. Since the corrosion tends to be uniformly distributed along the sample length with increasing level of corrosion, a better fitting of the experimental results is expected.
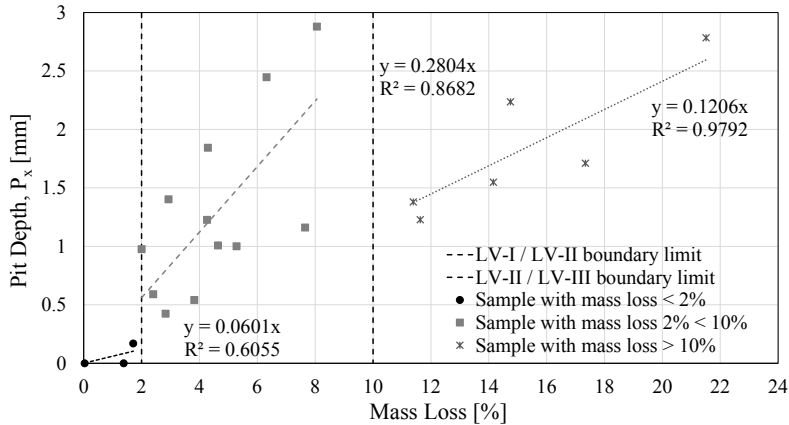
Figure 18. Correlation between maximum pit depth and mass loss of corroded samples.

A further attempt to evaluate strand deterioration consisted in the use of the residual cross-sectional area. Figure 19 reports the correlation between the ratio of the corroded and uncorroded cross-sectional area and the percentage of mass loss of the collected samples. In the case study, the residual cross-sectional area has been evaluated considering both the minimum, A_{min}, and the average, A_{av}, values. The correlation coefficient, R^2, equal to 0.8774 and 0.9126 in case of minimum and average cross-sectional area, respectively, highlights good inversely linear relationships for both case studies. This outcome is consistent with the results obtained by Li et al. [27], Kashani et al. [43], and Tang et al. [44] for the corrosion of reinforcing steel bars in a chloride environment and deformed steel bars in concrete, respectively. Adopting the same procedure for prestressing strands, the graph plotted in Figure 19 has been obtained. Therefore, it is possible to assess that the residual cross-sectional area is a relevant material damage parameter for prestressing strands characterised by chloride-induced corrosion.

16
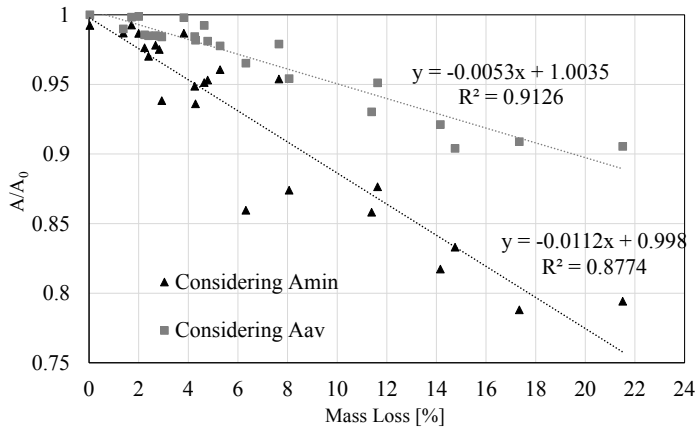
Figure 19. Correlation between residual cross-sectional area and mass loss.

4.3 Pitting Factor

In the last years, controversial intervals of pitting factor, P_f, have been obtained for reinforcing steel bars by different authors [19]-[25]. In this paper, additional data are recorded in order to extend the available experimental results and to promote scientific research in case of prestressing steel.

As defined by Tuutti [19] and according to Zhao et al. [37], the pitting factor, P_f, is calculated as the ratio between the maximum pit depth, P_x, and the average corrosion depth, P_{av}. As first attempt, the average corrosion depth, $P_{av,1}$, along the entire length of the sample has been evaluated as a function of the calculated mass loss, η, according to the general expression reported in Eq.(10), which is directly obtained from Eq.(2), [45]:

$$P_{av,1} = \left(\frac{D}{2}\right)\left(1-\left[1-\eta/100\right]^{0.5}\right) \tag{10}$$

where, D is the equivalent strand diameter, assumed equal to 12.9 mm.

Subsequently, in order to correlate the overall response of the strand with the contributions provided by the external wires, a different measurement of the average pit depth, $P_{av,2}$, considered as the average value of the maximum pit depths recorded for each external wire, has been taken into account. The obtained values for both the analysed cases are summarised in Table 6.

Table 6. Pitting factor evaluation.

Identifying Code	P_x [mm]	$P_{av,1}$ [mm]	$P_{f,1}$ [-]	$P_{av,2}$ [mm]	$P_{f,2}$ [-]
PB9-R(15-60)	2.7846	0.7353	3.79	1.668	1.67
PB9-R(428-473)	0.1697	0.0554	3.06	0.1697	1.00
PB9-L(12-82)	1.7112	0.5844	2.93	1.37	1.25
PB9-L(426-496)	0.4238	0.0909	4.66	0.405	1.05
PB10-R(287-332)	2.88	0.2634	10.93	1.508	1.91
PB10-L(138-208)	0.5905	0.0779	7.58	0.262	2.25
PB10-L(445-515)	2.4468	0.2071	11.81	1.705	1.44
PB11-R(6-51)	0.9757	0.0648	15.05	0.449	2.17
PB11-L(196-266)	1.4022	0.0942	14.88	0.72	1.95
PB12-R(100-170)	1.0013	0.1733	5.78	0.831	1.20
PB12-L(12-82)	1.5491	0.4755	3.26	1.066	1.45
PB12-L(124-169)	1.2274	0.1402	8.75	0.795	1.54
PB13-R(0-70)	1.3798	0.3788	3.64	1.194	1.16
PB13-R(70-115)	1.0083	0.1501	6.72	0.686	1.47
PB13-L(1-46)	1.4619	0.2499	5.85	0.999	1.46
PB13-L(108-178)	1.8433	0.1402	13.15	1.496	1.23
PB14-R(2-72)	1.2275	0.3856	3.18	1.163	1.06
PB14-R(77-122)	0.5414	0.1237	4.38	0.438	1.24
PB14-L(10-55)	2.2368	0.4929	4.54	1.466	1.53

17

Referring to the average pit depth, $P_{av,1}$, calculated as a function of the mass loss, the pitting factor data points, $P_{f,1}$, are distributed in the interval of 2.93 to 15.05, as highlighted in Figure 20. This range of values is comparable with the interval recorded by Gonzalez et al. [21] in case of reinforcing rebars. However, a widespread interval of values is obtained if compared with the range recorded by Darmawan and Stewart [30] (2.7-8.9) in case of prestressing wires. The discrepancy in the range can be attributed to the corrosion process taken into account (natural instead of accelerated) and to the higher number of samples analysed in the present study.
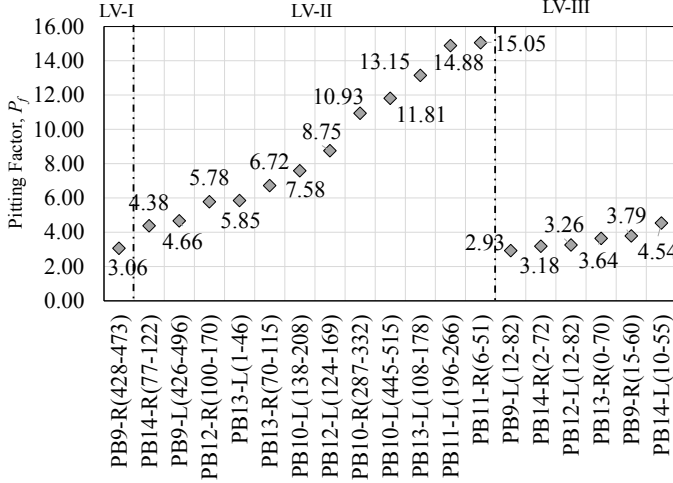
Figure 20. Distribution of pitting factor, referring to $P_{av,1}$.

On the other hand, the relationship between the average, $P_{av,2}$, and the maximum pit depth, P_x, has been evaluated and reported in Figure 21. The outcomes reveal that, regardless of the level of corrosion of the samples, the trend of the data distribution could be well interpolated by a linear function, as shown in Figure 21 and by Eq.(11):

$$P_{av,2} = 0.6638 \cdot P_x \tag{11}$$

The average value of R^2 for all the samples is 0.969 which reflects a good correlation between the fitting line and the experimental data. According to Figure 21, it is possible to point out that generally the maximum pit depth constantly increases with the growth of the steel corrosion. These outcomes are in line with the results obtained by Zhao et al. [37] for reinforcing rebars, who also observed that, for pitting corrosion, the maximum pit depth results always greater than the average pit depth.

   Firstly, Eq.(7)-(9) are used with the aim to relate the mass loss with the maximum pit depth, and secondly Eq.(11) provides the relationship between the average and maximum pit depth, respectively. In general, by means of Eq.(11), an indirect measurement of the average pit depth, $P_{av,2}$, can be estimated. This value could be potentially relevant for a preliminary assessment of the corrosion deterioration.
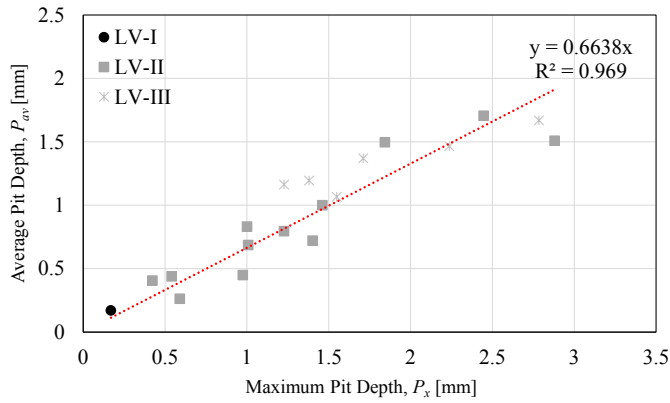
Figure 21. Relationship between the average and the maximum pit depth.

The pitting factor, $P_{f,2}$, is plotted in Figure 22, where the dashed red line indicates that the maximum pitting corrosion depth is approximately 1.5 times the average corrosion depth, $P_{av,2}$. This value corresponds to the inverse value of the slope of Eq.(11).

In Figure 22, the data points are mainly distributed in the interval of 1.05 to 2.17, except sample PB9-R(428-473), equal to 1.00, and sample PB10-L(138-208), equal to 2.25. For sample PB9-R(428-473) characterised by a small pitting factor, a small pit appears on the upper side of the external surface. Since only a single pit has been detected, the maximum pit corresponds to the average pit value and then the pitting factor results to be equal to 1. Sample PB10-L(138-208) was characterised by the largest pitting factor. In this sample, three external wires are classified as uncorroded, while the remaining three show a low level of corrosion along the sample length with pits depth ranging from 0.1 mm to 0.4 mm. Since the high corrosion area is localised in a single wire, showing only one deep pit equal to 0.59 mm, the maximum pit depth is approximately 2.25 times the value of the average pit depth.
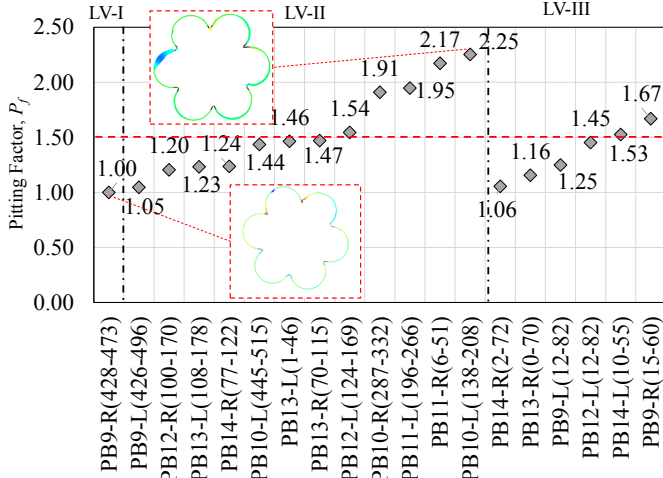
Figure 22. Distribution of pitting factor, referring to $P_{av,2}$.

Finally, the Cumulative Distribution Function, CDF, is plotted in Figure 23. Since it is generally recognised that the higher pit depths have the most detrimental effect on the wire and on the overall structural capacity of the strand, the Normal, Lognormal, and Gumbel distributions are considered for the fitting of the measured maximum pit depth data, as shown in Figure 23. In particular, the maximum pit depths recorded for the 19 corroded samples are grouped into predefined intervals, with a size of 0.2 mm. Table 7 reports the summary of all the statistical parameters taken into account. As first step, a bar graph - histogram - has been obtained based on the number of observations in each interval, by counting the number of the observed values that fall into each interval. In this step, by looking at the bar graph, a first visual determination in the trend of data has been achieved. Then, once the relative frequency of

19

occurrence, defined as the ratio between the total number of observations for the interval and the total number of all observations, has been calculated, see Figure 23, the cumulative frequency has been evaluated by adding up the frequency value for the analysed interval and all the previous one. As a result, as already observed by Darmawan and Stewart [30] for the evaluation of the pitting factor considering a single wire, the distribution of maximum pit depth can be best interpolated by using the Gumbel extreme value (EV-type I) distribution. For the present study, the statistical parameters in terms of average and standard deviation are equal to 1.414 and 0.769, respectively.
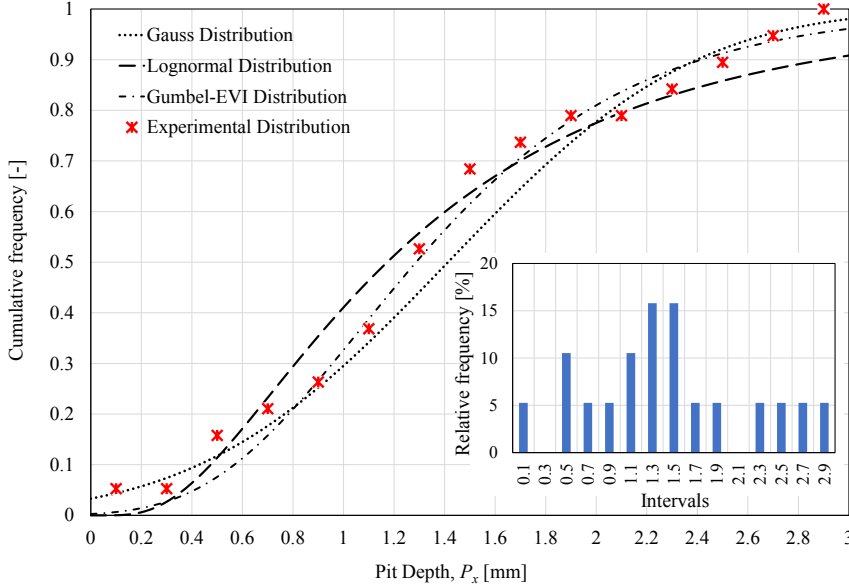
Figure 23. Statistical Investigation of maximum pit depth, P_x.

Table 7. Statistical Parameters

Range	Number of observations in interval	Frequency of occurrence	Cumulative Frequency
0 - 0.2	1	0.0526	0.0526316
0.2 - 0.4	0	0	0.0526316
0.4 - 0.6	2	0.1052	0.1578947
0.6 - 0.8	1	0.0526	0.2105263
0.8 -1.0	1	0.0526	0.2631579
1.0 -1.2	2	0.1052	0.3684211
1.2 -1.4	3	0.1578	0.5263158
1.4 -1.6	3	0.1578	0.6842105
1.6 -1.8	1	0.0526	0.7368421
1.8 -2.0	1	0.0526	0.7894737
2.0 -2.2	0	0	0.7894737
2.2 -2.4	1	0.0526	0.8421053
2.4 -2.6	1	0.0526	0.8947368
2.6 -2.8	1	0.0526	0.9473684
2.8 -3.0	1	0.0526	1

5 CONCLUSIONS

In the present work, in order to evaluate the effects of chloride-induced corrosion on prestressing strands and to extend the available experimental results concerning PC structures, 24 samples - retrieved from six naturally corroded PC beams - have been analysed. After the scanning phase and the post-processing of data performed by using GOM Inspect software, the maximum pits associated to each external wire have been classified according to the pit type configurations provided by Jeon et al. [34]. Then, based on the uncertainty of the in-situ measurements, a univocal expression for the calculation of the area of

pits, belonging to type 1 and type 3 has been suggested. Finally, starting from the mass loss calculation, an approximate method for the evaluation of the average pit depth of a prestressing strand in case of different levels of corrosion has been proposed.

The main concluding remarks of the study are the following:

I. The pit depth and the residual cross-sectional area of corroded samples are irregularly distributed along the length of prestressing strands. Outcomes reveal that the maximum pit depth and the residual cross-sectional area increase and decrease with increased levels of corrosion, respectively.

II. Referring to the 101 pits classified according to three types of pit configuration [34], 46.5% and 47.5% of the analysed pits belong to type 1 and type 3, respectively, while the remaining 6% belongs to type 2. In particular, pits classified as type 2 have been recorded only in the case of a high level of corrosion, LV-III, while pits classified as type 1 and type 3 occurred randomly regardless of the level of corrosion.

III. Since, especially considering a high level of corrosion, a univocal classification of pits in type 1 or 3 is almost not achievable during an in-situ inspection due to the high similarity in pit shapes, the use of type 3 expression is suggested for the evaluation of the pit area for both configurations. Outcomes reveal that a good interpolation of the experimental data is obtained.

IV. Based on the mass losses evaluated according to the gravimetrical method [40], a new method for the evaluation of the sample average pit depth is proposed.

V. Referring to experimental results, the interval of the pitting factor, P_f, in case of naturally corroded prestressing strand, fluctuates within 2.93 to 15.05 or within 1.05 to 2.17 for different pit shapes considering the average pit depth as a function of the calculated mass loss of the strand, $P_{av,1}$, or as the average value of the maximum pit depths recorded for each external wire, $P_{av,2}$, respectively.

Additional efforts will be devoted in future research to the investigation of interface imperfections between concrete and prestressing steel. In particular, a first observation immediately after the retrieval of corroded prestressing strands and another by using microscope analysis will be taken into account.

DECLARATION OF COMPETING INTEREST

The authors declare that they have no known competing financial interests or personal relationships that could have appeared to influence the work reported in this paper.

CRediT AUTHORSHIP CONTRIBUTION STATEMENT

Francesca Vecchi: Methodology, Visualization, Data curation, Conceptualization. **Lorenzo Franceschini:** Writing - original draft, Visualization, Data curation, Conceptualization. **Francesco Tondolo:** Supervision, Funding acquisition, Resources, Investigation. **Beatrice Belletti:** Project administration, Supervision, Writing - review editing, Conceptualization, Funding acquisition. **Javier Sánchez Montero:** Investigation, Validation. **Paolo Minetola:** Investigation, Data Curation, Writing - review editing.

ACKNOWLEDGEMENTS

DATA AVAILABILITY

The raw/processed data required to reproduce these findings cannot be shared at this time as the data also forms part of an ongoing study.

APPENDIX A

Considering the 24 collected samples, the following Table reports the geometrical description and classification of the maximum pit for each external wire (six for each sample) forming the strand.

Identifying Code		P_x [mm]	P_y [mm]	P_z [mm]	A_p [mm²]	$A_{p,1}$ [mm²]	$A_{p,2}$ [mm²]	$A_{p,3}$ [mm²]	Classification according to Jeon et al. [34]
PB9-L(12-82)	W_1	1.198	20.29	1.98	3.87	2.44	5.03	3.28	3
	W_2	1.336	27.03	2.36	3.98	2.86	5.59	3.82	3
	W_3	1.421	20.80	2.06	4.25	3.12	5.93	4.16	3
	W_4	1.144	6.52	2.81	2.45	2.28	4.81	3.08	1
	W_5	1.410	5.89	2.38	3.15	3.09	5.89	4.12	1
	W_6	1.711	25.63	2.28	5.76	4.08	7.08	5.35	3
PB9-L(426-496)	W_1	-	-	-	-	-	-	-	-
	W_2	-	-	-	-	-	-	-	-
	W_3	0.414	1.22	1.16	0.57	0.51	1.76	0.71	1
	W_4	0.424	0.73	0.83	0.51	0.53	1.80	0.74	1
	W_5	-	-	-	-	-	-	-	-
	W_6	0.377	1.95	1.31	0.49	0.44	1.60	0.62	1
PB9-R(15-60)	W_1	1.574	18.97	2.33	5.46	3.62	6.54	4.78	3
	W_2	1.620	12.84	2.41	5.83	3.77	6.72	4.97	2
	W_3	1.432	15.26	2.06	3.97	3.16	5.98	4.20	3
	W_4	2.785	13.78	2.87	9.21	8.09	10.94	9.86	3
	W_5	1.393	13.41	2.81	3.84	3.03	5.82	4.05	3
	W_6	1.202	8.93	1.42	3.53	2.45	5.05	3.30	3
PB9-R(428-473)	W_1	-	-	-	-	-	-	-	-
	W_2	-	-	-	-	-	-	-	-
	W_3	-	-	-	-	-	-	-	-
	W_4	0.170	1.86	0.65	0.11	0.14	0.72	0.19	1
	W_5	-	-	-	-	-	-	-	-
	W_6	-	-	-	-	-	-	-	-
PB10-L(138-208)	W_1	-	-	-	-	-	-	-	-
	W_2	0.317	3.52	1.43	0.52	0.34	1.35	0.48	3
	W_3	0.591	5.87	2.56	1.35	0.91	2.50	1.19	3
	W_4	0.405	4.76	1.68	0.68	0.41	1.72	0.69	3
	W_5	-	-	-	-	-	-	-	-
	W_6	-	-	-	-	-	-	-	-
PB10-L(445-515)	W_1	0.889	5.32	2.23	2.16	1.58	3.75	2.15	3
	W_2	1.166	4.16	2.08	3.59	2.35	4.90	3.16	3
	W_3	1.110	5.11	2.09	2.25	2.18	4.67	2.95	1
	W_4	2.447	8.39	3.56	7.78	6.76	9.80	8.46	3
	W_5	2.050	10.20	2.93	6.15	5.28	8.37	6.78	3
	W_6	2.566	15.03	3.69	7.36	7.23	10.22	8.96	1
PB10-R(32-102) **Uncorroded**	W_1	-	-	-	-	-	-	-	-
	W_2	-	-	-	-	-	-	-	-
	W_3	-	-	-	-	-	-	-	-
	W_4	-	-	-	-	-	-	-	-
	W_5	-	-	-	-	-	-	-	-
	W_6	-	-	-	-	-	-	-	-
PB10-R(287-332)	W_1	1.529	8.93	2.77	4.00	3.47	6.36	4.60	1
	W_2	1.360	6.32	2.87	4.51	2.93	5.69	3.92	3
	W_3	0.727	1.68	0.91	1.36	1.17	3.08	1.61	1
	W_4	1.426	7.22	2.96	3.94	3.14	5.95	4.18	3
	W_5	2.880	10.17	2.95	8.41	8.47	11.24	10.24	1
	W_6	1.127	7.31	1.69	1.85	2.23	4.74	3.01	1
PB11-L(5-75) **Uncorroded**	W_1	-	-	-	-	-	-	-	-
	W_2	-	-	-	-	-	-	-	-
	W_3	-	-	-	-	-	-	-	-
	W_4	-	-	-	-	-	-	-	-
	W_5	-	-	-	-	-	-	-	-
	W_6	-	-	-	-	-	-	-	-
PB11-L(196-266)	W_1	0.521	3.01	1.78	0.60	0.72	2.21	1.00	1

	W_2	0.898	5.99	2.90	2.30	1.60	3.79	2.19	3
	W_3	1.402	8.75	3.09	4.38	3.06	5.86	4.08	3
	W_4	0.505	2.66	1.08	0.35	0.68	2.14	0.95	1
	W_5	0.555	2.77	1.46	0.53	0.79	2.36	1.09	1
	W_6	0.437	1.09	1.42	0.52	0.55	1.86	0.77	1
PB11-R(6-51)	W_1	0.976	4.24	2.11	2.15	1.81	4.11	2.46	3
	W_2	-	-	-	-	-	-	-	-
	W_3	0.196	1.35	0.71	0.19	0.17	0.83	0.24	1
	W_4	-	-	-	-	-	-	-	-
	W_5	0.349	2.51	1.27	0.62	0.40	1.48	0.55	3
	W_6	0.274	2.41	0.76	0.25	0.28	1.17	0.39	1
PB11-R(273-318) (NEGLECTED)	W_1	-	-	-	-	-	-	-	-
	W_2	-	-	-	-	-	-	-	-
	W_3	1.152	14.22	3.40	2.91	2.30	4.84	3.11	3
	W_4	-	-	-	-	-	-	-	-
	W_5	-	-	-	-	-	-	-	-
	W_6	-	-	-	-	-	-	-	-
PB12-L(12-82)	W_1	1.549	15.47	3.89	4.82	3.54	6.44	4.68	3
	W_2	0.814	23.38	2.05	2.11	1.39	3.44	1.90	3
	W_3	1.075	10.32	1.97	2.39	2.08	4.52	2.82	1
	W_4	0.974	4.13	1.22	2.51	1.80	4.11	2.45	3
	W_5	0.734	6.51	2.00	2.94	1.19	3.11	1.64	2
	W_6	1.251	41.21	2.47	5.88	2.60	5.25	3.49	2
PB12-L(124-169)	W_1	0.645	2.61	1.70	1.53	0.98	2.73	1.36	3
	W_2	0.865	3.90	1.12	1.58	1.52	3.66	2.07	1
	W_3	0.958	13.25	3.28	2.12	1.76	4.04	2.40	3
	W_4	0.478	3.19	1.12	0.61	0.63	2.03	0.88	1
	W_5	0.599	4.91	1.63	0.66	0.88	2.54	1.22	1
	W_6	1.227	10.84	2.88	3.17	2.53	5.15	3.40	3
PB12-R(100-170)	W_1	0.894	4.68	1.52	1.96	1.59	3.77	2.17	3
	W_2	1.001	6.80	2.26	2.81	1.88	4.22	2.55	3
	W_3	0.766	2.67	2.67	1.40	1.27	3.24	1.74	1
	W_4	0.866	2.83	1.62	1.62	1.52	3.66	2.08	1
	W_5	0.782	11.03	1.74	1.20	1.31	3.31	1.79	1
	W_6	0.677	4.40	2.02	0.90	1.06	2.87	1.46	1
PB12-R(358-403) Uncorroded	W_1	-	-	-	-	-	-	-	-
	W_2	-	-	-	-	-	-	-	-
	W_3	-	-	-	-	-	-	-	-
	W_4	-	-	-	-	-	-	-	-
	W_5	-	-	-	-	-	-	-	-
	W_6	-	-	-	-	-	-	-	-
PB13-L(1-46)	W_1	0.792	7.26	2.95	2.17	1.33	3.35	1.83	3
	W_2	0.724	8.68	2.00	1.72	1.17	3.07	1.61	3
	W_3	0.883	4.90	1.55	1.12	1.56	3.73	2.13	1
	W_4	1.462	7.52	1.62	2.06	3.25	6.10	4.32	1
	W_5	1.162	6.44	2.23	2.50	2.33	4.88	3.15	1
	W_6	0.972	5.77	1.41	2.97	1.80	4.10	2.45	3
PB13-L(108-178)	W_1	1.595	15.16	2.55	4.68	3.69	6.62	4.87	3
	W_2	1.286	21.60	2.90	2.60	2.70	5.39	3.62	1
	W_3	1.840	12.09	3.00	3.79	4.53	7.58	5.89	1
	W_4	1.327	8.21	3.60	3.69	2.83	5.55	3.78	3
	W_5	1.285	13.38	2.70	2.49	2.70	5.38	3.62	1
	W_6	1.645	15.23	3.36	4.12	3.86	6.82	5.07	1
PB13-R(0-70)	W_1	1.147	19.22	1.63	3.18	2.29	4.82	3.09	3
	W_2	1.297	4.57	1.91	2.82	2.74	5.43	3.67	1
	W_3	1.294	10.42	2.32	2.90	2.73	5.42	3.66	1
	W_4	1.141	9.53	1.74	2.44	2.27	4.80	3.07	1
	W_5	1.380	10.39	2.39	3.19	2.99	5.77	4.00	1
	W_6	0.908	6.81	1.39	3.12	1.63	3.83	2.22	2
PB13-R(70-115)	W_1	0.876	25.39	2.93	2.53	1.54	3.70	2.11	3
	W_2	1.008	12.01	2.84	2.80	1.90	4.25	2.58	3
	W_3	0.779	7.85	2.33	2.16	1.30	3.30	1.78	3
	W_4	0.465	4.27	1.86	0.92	0.61	1.97	0.84	3

	W_5	0.634	2.58	1.39	1.02	0.96	2.69	1.32	1
	W_6	0.353	3.63	1.61	0.53	0.40	1.50	0.56	1
PB14-L(10-55)	W_1	2.229	34.19	2.97	7.58	5.94	9.03	7.54	3
	W_2	1.099	5.79	1.73	2.92	2.15	4.62	2.91	3
	W_3	1.290	10.91	2.16	3.08	2.72	5.40	3.64	1
	W_4	2.237	17.51	3.43	5.92	5.97	9.06	7.57	1
	W_5	0.837	16.38	2.40	2.93	1.44	3.54	1.98	2
	W_6	1.106	3.51	2.45	3.88	2.17	4.65	2.93	2
PB14-L(455-500)	W_1	-	-	-	-	-	-	-	-
Uncorroded	W_2	-	-	-	-	-	-	-	-
	W_3	-	-	-	-	-	-	-	-
	W_4	-	-	-	-	-	-	-	-
	W_5	-	-	-	-	-	-	-	-
	W_6	-	-	-	-	-	-	-	-
PB14-R(2-72)	W_1	1.201	16.49	1.76	1.93	2.45	5.04	3.30	1
	W_2	1.055	17.58	2.42	3.08	2.03	4.44	2.75	3
	W_3	1.228	10.19	2.32	2.63	2.53	5.15	3.40	3
	W_4	1.180	5.26	1.20	2.91	2.38	4.95	3.21	3
	W_5	1.095	19.40	2.23	3.64	2.14	4.61	2.90	3
	W_6	1.217	27.04	2.24	3.04	2.50	5.11	3.36	3
PB14-R(77-122)	W_1	0.481	3.35	1.40	0.58	0.64	2.04	0.88	1
	W_2	0.424	3.58	1.28	0.40	0.53	1.80	0.74	1
	W_3	0.413	0.94	0.61	0.38	0.51	1.75	0.71	1
	W_4	0.329	1.99	1.38	0.52	0.36	1.40	0.51	3
	W_5	0.443	5.45	1.06	0.62	0.56	1.88	0.78	1
	W_6	0.541	2.53	0.96	0.71	0.76	2.30	1.05	1

** Where W stands for wire and the number ranging from 1 to 6 identifies the numbering of external wires.

APPENDIX B

Identifying Code	Wire	A_p [mm²]	Type 3 Jeon et al. [34]	
			Area [mm²]	error committed [%]
PB9-L(12-82)	W_1	3.87	3.28	15.25
	W_2	3.98	3.82	3.91
	W_3	4.25	4.16	2.14
	W_4	2.45	3.08	-25.72
	W_5	3.15	4.12	-30.78
	W_6	5.76	5.35	7.14
PB9-L(426-496)	W_1	-	-	-
	W_2	-	-	-
	W_3	0.57	0.71	-23.82
	W_4	0.51	0.74	-43.44
	W_5	-	-	-
	W_6	0.49	0.62	-27.13
PB10-L(445-515)	W_1	2.16	2.15	0.03
	W_2	3.59	3.16	11.99
	W_3	2.25	2.95	-31.37
	W_4	7.78	8.46	-8.83
	W_5	6.15	6.78	-10.32
	W_6	7.36	8.96	-21.74
PB11-R(6-51)	W_1	2.15	2.46	-14.62
	W_2	-	-	-
	W_3	0.19	0.24	-22.34
	W_4	-	-	-
	W_5	0.62	0.55	11.25
	W_6	0.25	0.39	-52.83
PB11-L(196-266)	W_1	0.60	1.00	-65.37
	W_2	2.30	2.19	4.79
	W_3	4.38	4.08	6.67
	W_4	0.35	0.95	-170.58
	W_5*	**0.53**	**-**	**-**
	W_6*	**0.52**	**-**	**-**
PB12-L(12-82)	W_1	4.82	4.68	3.00
	W_2	2.11	1.90	9.95
	W_3	2.39	2.82	-17.88
	W_4	2.51	2.45	2.40
	W_5	2.94	1.64	44.30
	W_6	5.88	3.49	40.63
PB10-L(138-208)	W_1	-	-	-
	W_2	0.52	0.48	7.29
	W_3	1.35	1.19	11.39
	W_4	0.68	0.69	-1.33
	W_5	-	-	-
	W_6	-	-	-
PB12-R(100-170)	W_1	1.96	2.17	-10.61
	W_2	2.81	2.55	9.08
	W_3	1.40	1.74	-23.90
	W_4	1.62	2.08	-28.44
	W_5	1.20	1.79	-49.02
	W_6	0.90	1.46	-61.12
PB13-L(1-46)	W_1	2.17	1.83	15.79
	W_2	1.72	1.61	6.56
	W_3	1.12	2.13	-90.88
	W_4	2.06	4.32	-110.30
	W_5	2.50	3.15	-26.06
	W_6	2.97	2.45	17.67
PB13-L(108-178)	W_1	4.68	4.87	-3.97
	W_2	2.60	3.62	-39.18
	W_3	3.79	5.89	-55.53

	W_4	3.69	3.78	-2.58
	W_5	2.49	3.62	-45.52
	W_6	4.12	5.07	-23.03
PB13-R(0-70)	W_1	3.18	3.09	2.85
	W_2	2.82	3.67	-30.05
	W_3	2.90	3.66	-25.92
	W_4	2.44	3.07	-25.59
	W_5	3.19	4.00	-25.15
	W_6*	**3.12**	**-**	**-**
PB13-R(70-115)	W_1	2.53	2.11	16.57
	W_2	2.80	2.58	7.91
	W_3	2.16	1.78	17.33
	W_4	0.92	0.84	8.72
	W_5	1.02	1.32	-29.40
	W_6	0.53	0.56	-5.72
PB14-L(10-55)	W_1	7.58	7.54	0.54
	W_2	2.92	2.91	0.28
	W_3	3.08	3.64	-18.22
	W_4	5.92	7.57	-27.86
	W_5*	**2.93**	**-**	**-**
	W_6*	**3.88**	**-**	**-**
PB14-R(77-122)	W_1	0.58	0.88	-51.84
	W_2	0.40	0.74	-81.77
	W_3	0.38	0.71	-86.78
	W_4	0.52	0.51	2.06
	W_5	0.62	0.78	-26.32
	W_6	0.71	1.05	-47.43
PB14-R(2-72)	W_1	1.93	3.30	-70.52
	W_2	3.08	2.75	10.86
	W_3	2.63	3.40	-29.19
	W_4	2.91	3.21	-10.31
	W_5	3.64	2.90	20.40
	W_6	3.04	3.36	-10.48
PB9-R(15-60)	W_1	5.46	4.78	12.35
	W_2*	**5.83**	**-**	**-**
	W_3	3.97	4.20	-6.01
	W_4	9.21	9.86	-7.05
	W_5	3.84	4.05	-5.40
	W_6	3.53	3.30	6.52
PB9-R(428-473)	W_1	-	-	-
	W_2	-	-	-
	W_3	-	-	-
	W_4	0.11	0.19	-77.03
	W_5	-	-	-
	W_6	-	-	-
PB10-R(287-332)	W_1	4.00	4.60	-14.94
	W_2	4.51	3.92	13.11
	W_3	1.36	1.61	-18.60
	W_4	3.94	4.18	-6.18
	W_5	8.41	10.24	-21.87
	W_6	1.85	3.01	-63.12
PB12-L(124-169)	W_1	1.53	1.36	11.16
	W_2	1.58	2.07	-31.21
	W_3	2.12	2.40	-13.13
	W_4	0.61	0.88	-43.81
	W_5	0.66	1.22	-84.04
	W_6	3.17	3.40	-7.23

*In bold the wires classified as type 2 – Not considered in the comparison.

7
8

REFERENCES

[1]	K. Asami, M. Kikuchi, In-depth distribution of rusts on a plain carbon steel and weathering steels exposed to coastal-industrial atmosphere for 17 years, Corrosion Science. 45 (2003) 2671-2688. https://doi.org/10.1016/S0010-938X(03)00070-2

[2]	Y. Zhao, B. Hu, J. Yu, W. Jin, Non-uniform distribution of rust layer around steel bar in concrete, Corrosion Science. 53(2011) 4300-4308. https://doi.org/10.1016/j.corsci.2011.08.045

[3]	Z.h. Lu, F. Li, Y.G. Zhao, An investigation of degradation of mechanical behaviour of pre-stressing strands subjected to chloride attacking, 5th International Conference on Durability of Concrete Structures, Jun 30 – Jul 1, 2016. Shenzhen University, Shenzhen, Guangdong Province, China.

[4]	J.P. Bhargava, A.K. Ghosh, Y. Mori, S. Ramanujam, Corrosion-induced bond strength degradation in reinforced concrete – Analytical and empirical models, Nuclear Engineering and Design. 237(2007) 1140-1157. https://doi.org/10.1016/j.nucengdes.2007.01.010

[5]	B.S. Jang, B.H. Oh, Effects of non-uniform corrosion on the cracking and service life of reinforced concrete structures, Cement and Concrete Research. 40(2010) 1441-1450. https://doi.org/10.1016/j.cemconres.2010.03.018

[6]	C. Cao, M.M.S. Cheung, B.Y.B. Chan, Modelling of interaction between corrosion-induced concrete cover crack and steel corrosion rate, Corrosion Science. 69(2013) 97-109. https://doi.org/10.1016/j.corsci.2012.11.028

[7]	S. Yoon, K.J. Wang, K.J. Weiss, S.P. Shah, Interaction between loading, corrosion, and serviceability of reinforced concrete, ACI Material Journal. 97(2000) 637-644.

[8]	R. Zhang, A. Caste, R. Francois, The corrosion pattern of reinforcement and its influence on serviceability of reinforced concrete members in chloride environment, Cement and Concrete Research. 39(2009) 1077-1086. https://doi.org/10.1016/j.cemconres.2009.07.025

[9]	F. Li, Y. Yuan, C.Q. Li, Corrosion propagation of prestressing steel strands in concrete subject to chloride attack, Construction and Building Material. 25(2011) 3878–3885. https://doi.org/10.1016/j.conbuildmat.2011.04.011

[10]	B. Belletti, F. Vecchi, C. Bandini, C. Andrade, J. Sanchez, Numerical evaluation of the corrosion effects in prestressed concrete beams without shear reinforcement, Structural Concrete. 21(2020) 1794-1809. https://doi.org/10.1002/suco.201900283

[11]	B. Belletti, J. Rodrìguez, C. Andrade, L. Franceschini, J. Sànchez Montero, F. Vecchi, Experimental tests on shear capacity of naturally corroded prestressed beams, Structural Concrete. 21(2020) 1777–1793. https://doi.org/10.1002/suco.202000205

[12]	M.G. Alvarez, J.R. Galvele, The mechanism of pitting of high purity iron in NaCl solutions, Corrosion Science. 24(1984) 27–48. https://doi.org/10.1016/0010-938X(84)90133-1

[13]	A. Turnbull, L.N. McCartney, S. Zhou, A model to predict the evolution of pitting corrosion and the pit-to-crack transition incorporating statistically distributed input parameters, Corrosion Science. 48(2006) 2084-2105. https://doi.org/10.1016/j.corsci.2005.08.010

[14]	J. Sanchez, J. Fullea, C. Andrade, Corrosion-induced brittle failure in reinforcing steel, Theoretical and Applied Fracture Mechanism. 92(2017) 229–232. https://doi.org/10.1016/j.tafmec.2017.08.006

[15]	M. Elices, A. Valiente, L. Caballero, M. Iordachescu, J. Fullea, J. Sánchez-Montero, V. López-Serrano, Failure analysis of prestressed anchor bars, Engineering Failure Analysis. 24(2012) 57–66. https://doi.org/10.1016/j.engfailanal.2012.03.007

[16]	E. Proverbio, G. Ricciardi, Failure of a 40 years old post-tensioned bridge near seaside, Proceedings of the International Conference Eurocorr, London, 2000.

[17]	D. Goins, Motor speedway bridge collapse caused by corrosion, Materials Performance. 39(2000):18-19.

[18]	K.C. Hover, Special problems in evaluating the safety of concrete bridges and concrete bridge components, Construction and Building Materials. 10(1996) 39-43. https://doi.org/10.1016/0950-0618(95)00059-3

[19]	K. Tuutti, Corrosion of steel in Concrete, Swedish Cement and Concrete, Research Institute, 1982.

[20]	C.A. Apostolopoulos, S. Demis, V.G. Papadakis, Chloride-induced corrosion of steel reinforcement – mechanical performance and pit depth analysis, Construction and Building Material. 38(2013) 139-146. https://doi.org/10.1016/j.conbuildmat.2012.07.087

[21] J.A. Gonzàlez, C. Andrade, C. Alonso, S. Feliu, Comparison of rates of general corrosion and maximum fitting penetration on concrete embedded steel reinforcement, Cement Concrete Resistance. 25(1995) 257-264. https://doi.org/10.1016/0008-8846(95)00006-2

[22] J. Rodriguez, L. Ortega, J. Casal, Load carrying capacity of concrete structures with corroded reinforcement, Construction and Building Material. 11(1997) 239-248. https://doi.org/10.1016/S0950-0618(97)00043-3

[23] A.A. Torres-Acosta, M. Martinéz-Madrid, Residual life of corroding reinforced concrete structures in marine environment, Journal of Materials in Civil Engineering. 15(2003) 344-353.

[24] A.A. Torres-Acosta, P. Castro-Borges, Corrosion-Induced Cracking of Concrete Elements Exposed to a natural Marine Environment for Five Years, Corrosion Science. 69(2013) 1122-1131. https://doi.org/10.5006/0844

[25] L. Yu, R. Francois, V.H. Dang, V. L'Hostis, R. Gagné, Distribution of corrosion and pitting factor of steel in corroded RC beams, Construction and Building Material. 95(2015)384-392. https://doi.org/10.1016/j.conbuildmat.2015.07.119

[26] I. Finozzi, A. Saetta, H. Budelmann, Structural response of reinforcing bars affected by pitting corrosion: experimental evaluation, Construction and Building Materials. 192(2018) 478-488. https://doi.org/10.1016/j.conbuildmat.2018.10.088

[27] D. Li, R. Wei, L. Li, X. Guan, X. Mi, Pitting corrosion of reinforcing steel bars in chloride contaminated concrete, Construction and Building Material. 199(2019) 359-368. https://doi.org/10.1016/j.conbuildmat.2018.12.003

[28] G. Mancini, F. Tondolo, L. Iuliano, P. Minetola, Local reinforcing bar damage in r.c. members due to accelerated corrosion and loading, Construction and Building Materials. 69(2014) 116-123. https://doi.org/10.1016/j.conbuildmat.2014.07.011

[29] C.H. Yoo, Y.C. Park, H.K. Kim, Section loss in naturally corroded 7-wire strands in external tendons, Structure and Infrastructure Engineering. 16(2020) 1593-1603. https://doi.org/10.1080/15732479.2020.1714668

[30] M.S. Darmawan, M.G. Stewart, Effect of pitting corrosion on capacity of prestressing wires, Magazine of Concrete Research. 59(2007) 131-139. https://doi.org/10.1680/macr.2007.59.2.131

[31] D.V. Val, R.E. Melchers, Reliability of deteriorating RC slab bridges, Journal of Structural Engineering. 123(1997) 1638-1644.

[32] Y. Huang, C. Wei, L. Chen, P. Li, Quantitative correlation between geometric parameters and stress concentration of corrosion pits, Engineering Failure Analysis. 44(2014) 168-178. https://doi.org/10.1016/j.engfailanal.2014.05.020

[33] J. Hou, L. Song, Numerical investigation on stress concentration of tension steel bars with one or two corrosion pits, Advances in Materials Science and Engineering. 2015:1-7. https://doi.org/10.1155/2015/413737

[34] C.H. Jeon, J.B. Lee, S. Lon, C.S. Shim, Equivalent material model of corroded prestressing steel strand, Journal of Materials Research and Technology. 8(2019) 2450-2460. https://doi.org/10.1016/j.jmrt.2019.02.010

[35] L. Wang, T. Li, L. Dai, W. Chen, K. Huang, Corrosion morphology and mechanical behavior of corroded prestressing strands, Journal of Advanced Concrete Technology. 18(2020) 545-557. https://doi.org/10.3151/jact.18.545

[36] W. Zhang, C. Li, X. Gu, Y. Zeng, Variability in cross-sectional areas and tensile properties of corroded prestressing wires, Construction and Building Material. 228(2019) 1-11. https://doi.org/10.1016/j.conbuildmat.2019.116830

[37] Y. Zhao, X. Xu, Y. Wang, J. Dong, Characteristics of pitting corrosion in an existing reinforced concrete beam exposed to marine environment, Construction and Building Material. 234(2020) 1-12. https://doi.org/10.1016/j.conbuildmat.2019.117392

[38] F. Vecchi, B. Belletti, L. Franceschini, C. Andrade, J. Rodrìguez, J. Sànchez Montero, Flexural tests on prestressed beams exposed to natural chloride action, Proceedings of the 2nd CACRCS Workshop Capacity Assessment of Corroded Reinforced Concrete Structures, Dec. 1st-4th, 2020.

[39] L. Iuliano, P. Minetola, Enhancing moulds manufacturing by means of reverse engineering, The International Journal of Advanced Manufacturing Technology. 43 (2009): 551-562. https://doi.org/10.1007/s00170-008-1739-3

720 [40] American Society of Testing and Materials. ASTM G1-03, Standard Practice for Preparing, Cleaning, and Evaluating Corrosion Test Specimens, ASTM International, Annual Book of ASTM Standards, Vol 03.02.

723 [41] A. Valor, F. Caleyo, D. Rivas, J.M. Hallen, Stochastic approach to pitting-corrosion-extreme modelling in low carbon steel, Corrosion Science. 52(2010) 910-915. https://doi.org/10.1016/j.corsci.2009.11.011

726 [42] N. Murer, R. Buchheit, Stochastic modeling of pitting corrosion in aluminium alloys, Corrosion Science. 69(2013) 139-148. https://doi.org/10.1016/j.corsci.2012.11.034

728 [43] M.M. Kashani, A.J. Crewe, N.A. Alexander, Use of a 3D optical measurement technique for stochastic corrosion pattern analysis of reinforcing bars subjected to accelerated corrosion, Corrosion Science. 73(2013) 208-221. https://doi.org/10.1016/j.corsci.2013.03.037

731 [44] F. Tabg, Z. Lin, G. Chen, W. Yi, Three-dimensional corrosion pit measurement and statistical mechanical degradation analysis of deformed steel bars subjected to accelerated corrosion, Construction and Building Material. 70(2014) 104-117. https://doi.org/10.1016/j.conbuildmat.2014.08.001

735 [45] J.A. Morales, J. Torres, N. Rebolledo, J. Sanchez, Experimental and statistical analysis of the corrosion in tendons in contact with water, Frontiers in Materials. 6(2019) 167. https://doi.org/10.3389/fmats.2019.00167

738